

## **A trapdoor mechanism for slab tearing and melt generation in the northern Andes**

Gideon Rosenbaum, Mike Sandiford, John Caulfield and Jennifer M Garrison

### **METHODS**

#### **Seismology**

Earthquake locations are derived from the ISC-EHB Bulletin, International Seismological Commission (<http://www.isc.ac.uk/isc-ehb>), and tension (T) axis trends from the Global CMT Project catalogue (Dziewonski et al., 1981; Ekström et al., 2012). Data from the ISC-EHB Bulletin are based on teleseismically well-constrained events for the period 1960–2008, relocated using the EHB algorithm (Engdahl et al., 1998). This algorithm minimizes errors in location and, particularly, depth. In Fig. 2B–D we also show the full ISC catalogue (M2.5+) for the region.

#### **Volcanism**

The locations of active and extinct volcanoes were taken from the Global Volcanism Program's website (Volcanoes of the World, v. 4.6.7, downloaded 1 March 2018).

#### **Geochemistry**

The Sumaco slab melting model is designed to reproduce the metasomatic and melting processes taking place in the sub-backarc mantle. All modelling was undertaken in Excel. Melt trace element concentrations were calculated using the batch melting equation of Shaw (1970). The model assumes 5% slab melting (Kay et al., 1993) in the garnet stability field in the presence of 60% garnet, 39.3% clinopyroxene, and 0.7% rutile (Xiong et al., 2005). A representative Carnegie Ridge basalt trace element composition (Harpp et al., 2004) and

mineral/melt partition coefficients (Xiong et al., 2005; Xiong, 2006) are presented in Table DR2. The slab melt is mixed with average DMM (Workman and Hart, 2005) based on isotopic constraints on Sumaco lavas (Ancellin et al., 2017). We employ a bulk mixture comprising 98% DMM and 2% slab melt. The proportion of slab melt added to the source is inferred to be small on account of the highly incompatible element enriched composition of the slab melt relative to the upper mantle (typically 2 – 3 orders of magnitude higher). This source mixture is then re-melted in the spinel stability field (<80 km depth) in accordance with the two-stage melting regime previously proposed for Sumaco (Garrison et al., 2018). Partition coefficients (Halliday et al., 1995; McDade et al., 2003), DMM modal assemblage (Falloon and Green, 1988) and melt reaction (Robinson et al., 1998) are included in Table DR2. The degree of melting is inferred to be very low ( $\leq 3\%$ ); at higher values, the concentrations of the most incompatible elements during mantle melting (e.g. Rb, Ba, Nb and Pb) decrease rapidly in the resulting melts and would thus plot well below the values shown for Sumaco (Fig. 3B). The arc front Atacazo model uses the same DMM upper mantle composition, but a lower extent of slab melting (3%). The Atacazo source comprises 93% DMM, 1% slab melt, 3% slab fluid and 3% sediment melt. The fluid composition was modelled through dehydration of Carnegie Ridge basalt (Harpp et al., 2004) calculated using a Rayleigh distillation and bulk distribution coefficients determined at 800°C, 4 GPa and  $F = 0.23$  (Kessel et al., 2005). The sediment melt was calculated using the sediment composition from DSDP site 504 (Plank and Langmuir, 1998) and crystal/melt distribution coefficients from 800°C sediment melting experiments (Johnson and Plank, 2000) (cf. Table DR2). Incompatible trace element data presented on Figure 3B are normalised using N-MORB values from Sun and McDonough (1989). On Figure 3C, the fractionation of orthopyroxene, plagioclase and ilmenite (mineral vectors not shown) have a negligible effect on Nb/Y and

La/Yb ratios. Published partition coefficients were taken from the GERM website

(<https://earthref.org/KDD/>) and are included in Table DR2.

## REFERENCES CITED

- Ancellin, M.-A., Samaniego, P., Vlastélic, I., Nauret, F., Gannoun, A., and Hidalgo, S., 2017, Across-arc versus along-arc Sr-Nd-Pb isotope variations in the Ecuadorian volcanic arc: *Geochemistry, Geophysics, Geosystems*, v. 18, p. 1163-1188.
- Dziewonski, A. M., Chou, T.-A., and Woodhouse, J. H., 1981, Determination of earthquake source parameters from waveform data for studies of global and regional seismicity: *Journal of Geophysical Research: Solid Earth*, v. 86, p. 2825–2852.
- Ekström, G., Nettles, M., and Dziewoński, A. M., 2012, The global CMT project 2004–2010: Centroid-moment tensors for 13,017 earthquakes: *Physics of the Earth and Planetary Interiors*, v. 200-201, p. 1–9.
- Engdahl, E. R., van der Hilst, R. D., and Buland, R., 1998, Global teleseismic earthquake relocation with improved travel times and procedures for depth determination: *Bulletin of the Seismological Society of America*, v. 88, p. 722–743.
- Falloon, T., and Green, D., 1988, Anhydrous partial melting of peridotite from 8 to 35 kb and the petrogenesis of MORB: *Journal of Petrology*, no. p. 379–414.
- Garrison, J.M., Sims, K.W.W., Yogodzinski, G.M., Escobar, R.D., Scott, S., Mothes, P., Hall, M.L., and Ramon, P., 2018, Shallow-level differentiation of phonolitic lavas from Sumaco Volcano, Ecuador: *Contributions to Mineralogy and Petrology*, v. 173, <https://doi.org/10.1007/s00410-017-1431-4>.
- Halliday, A. N., Lee, D.-C., Tommasini, S., Davies, G. R., Paslick, C. R., Fitton, J. G., and James, D. E., 1995, Incompatible trace elements in OIB and MORB and source enrichment in the sub-oceanic mantle: *Earth and Planetary Science Letters*, v. 133, p. 379–395.
- Harpp, K. S., Wanless, V. D., Otto, R. H., Hoernle, K., and Werner, R., 2004, The Cocos and Carnegie aseismic ridges: A trace element record of long-term plume–spreading center interaction: *Journal of Petrology*, v. 46, p. 109–133.
- Hayes, G., 2018, Slab2 - A Comprehensive Subduction Zone Geometry Model: U.S. Geological Survey data release, <https://doi.org/10.5066/F7PV6JNV>.

- Johnson, M. C., and Plank, T., 2000, Dehydration and melting experiments constrain the fate of subducted sediments: *Geochemistry, Geophysics, Geosystems*, v. 1, 1007, doi:10.1029/1999GC000014.
- Kay, S. M., Ramos, V., and Marquez, M., 1993, Evidence in Cerro Pampa volcanic rocks for slab-melting prior to ridge-trench collision in southern South America: *The journal of Geology*, v. 101, p. 703–714.
- Kessel, R., Schmidt, M. W., Ulmer, P., and Pettke, T., 2005, Trace element signature of subduction-zone fluids, melts and supercritical liquids at 120–180 km depth: *Nature*, v. 437, p. 724–727.
- McDade, P., Blundy, J. D., and Wood, B. J., 2003, Trace element partitioning on the Tinaquillo Lherzolite solidus at 1.5 GPa: *Physics of the Earth and Planetary Interiors*, v. 139, p. 129–147.
- Plank, T., and Langmuir, C. H., 1998, The chemical composition of subducting sediment and its consequences for the crust and mantle: *Chemical geology*, v. 145, p. 325–394.
- Robinson, J., Wood, B., and Blundy, J., 1998, The beginning of melting of fertile and depleted peridotite at 1.5 GPa: *Earth and Planetary Science Letters*, v. 155, p. 97–111.
- Shaw, D. M., 1970, Trace element fractionation during anatexis: *Geochimica et Cosmochimica Acta*, v. 34, p. 237–243.
- Sun, S. S., and McDonough, W. F., 1989, Chemical and isotopic systematics of oceanic basalts: implications for mantle composition and processes: Geological Society, London, Special Publications, v. 42, p. 313–345.
- Workman, R. K., and Hart, S. R., 2005, Major and trace element composition of the depleted MORB mantle (DMM): *Earth and Planetary Science Letters*, v. 231, p. 53–72.
- Xiong, X., Adam, J., and Green, T., 2005, Rutile stability and rutile/melt HFSE partitioning during partial melting of hydrous basalt: implications for TTG genesis: *Chemical Geology*, v. 218, p. 339–359.
- Xiong, X.-L., 2006, Trace element evidence for growth of early continental crust by melting of rutile-bearing hydrous eclogite: *Geology*, v. 34, p. 945–948.

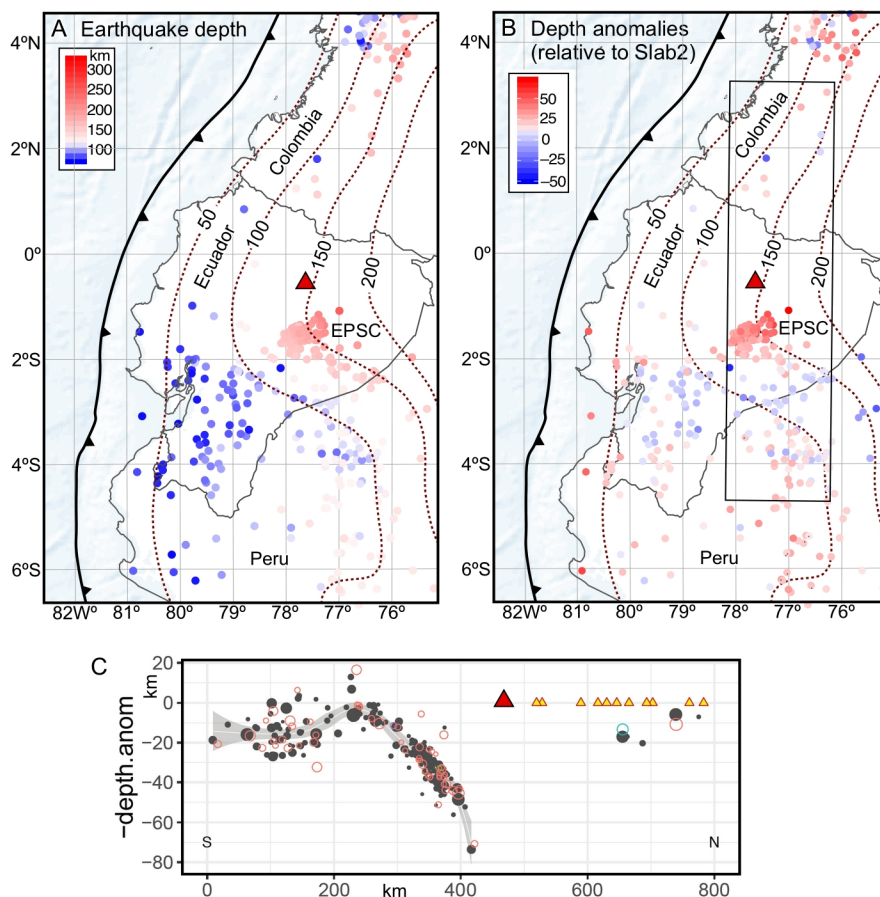


**Figure DR1.** A. Depth of ISC-EHB earthquakes (for events 70–340 km). B. Map highlighting areas where ISC-EHB hypocentres are deeper (red) and shallower (blue) than the Slab2 model (Hayes, 2018). Note that the colour axis is centered at 15 km beneath the Slab2 model top, because this is where maximum seismicity is expected. C. Cross section (see location in B) showing depth anomalies relative to Slab2 (Hayes, 2018). Note that substantial deviations occur immediately south of Sumaco Volcano (red triangle). EPSC, El Puyo Seismic Cluster.

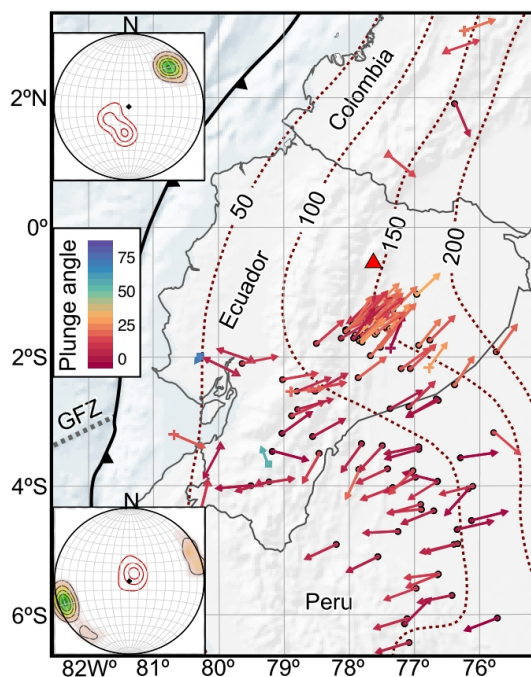


**Figure DR2.** CMT T-axes (for events > 70 km) with colours indicating plunge angle. The stereoplots show projected T-axes (black contours) and P-axes (red contours) for latitudes 6.5°–3°S (lower stereoplot) and 3°S–0° (upper stereoplot). Slab contours (in km) are based on the Slab2 model (Haynes, 2018). Red triangle indicates the location of Sumaco Volcano.

**Table DR1.** Extinct and active volcanoes in the Northern Andean Volcanic Zone

(2018418 Table DR1.xlsx)

**Table DR2.** Geochemical data and melting model calculation

(2018418 Table DR2.xlsx)